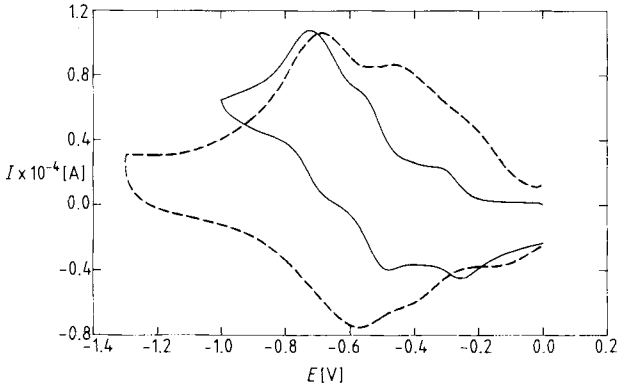

Fig. 1. Cyclovoltammograms of **1** and **4**. (– – –): Voltammogram of **1** embedded in a carbon paste electrode [12] in DMSO/0.1 M Bu_4NClO_4, scan rate 1 mV s^{-1}, E_p(red) = −0.20, −0.46, −0.69 V; E_p(ox) = −0.15, −0.41, −0.58 V. (— · —): Solution cyclic voltammogram of **4** in DMSO/0.1 M Bu_4NClO_4 on a 0.07 cm^2 Pt disk; scan rate 0.1 V s^{-1}, current scale in this case should be changed to 10^{-5}. Potentials are recorded vs. Ag/AgCl [3]. E_p(red) = −0.31, −0.55, −0.71 V; E_p(ox) = −0.26, −0.48, −0.68 V.

carbon paste electrode[12] (Fig. 1). The voltammogram is very similar to that of **4**. The further positive shift indicates more extended conjugation. The area under the slow sweep voltammogram in Figure 1 corresponds to 1.4 F mol^{-1} for both reduction and oxidation.

Polymer **1** is easily pressed into pellets which have an electrical conductivity[13] of $(1.3 \pm 0.2) \times 10^{-3}$ S cm^1. Neither the ESR spectrum nor the conductivity change on storage in air for two months. Likewise, **1** is stable in water and in many organic solvents. Exposure of the polymer to iodine vapors increases its conductivity by a factor of 2–3. Gaseous SO_2 has no effect. Doping experiments in solvent suspensions with I_2 and $FeCl_3$ for the oxidative process, or with $Na_2S_2O_4$ for the reductive process resulted in almost complete loss of conductivity. Thus, it appears that the necessary conditions for conductivity are produced during the dehydration process without the need for additional doping.

Received: January 27, 1989

[1] A. Diaz, J. Bargon in T. A. Skotheim (Ed.): *Handbook of Conducting Polymers*, Marcel Dekker, New York 1986, Vol. 1, p. 81.

[2] J. F. Fauvarque, M. A. Petit, A. Digue, G. Froyer, *Makromol. Chem. 188* (1987) 1833; R. B. Kaner, S. J. Porter, A. G. McDiarmid, *J. Chem. Soc., Faraday Trans. 82* (1986) 2323.

[3] The potentials reported were measured vs an AgCl coated silver wire in dimethyl sulfoxide (DMSO); the zero potential on this scale is 339 mV negative of the ferrocene signal.

[4] H. Simon, J. Bader, H. Günther, S. Neumann, J. Thanos, *Angew. Chem. Int. Ed. Engl. 24* (1985) 539; *Angew. Chem. 97* (1985) 541; L. Coche, J.-C. Moutet, *J. Electroanal. Chem. 224* (1987) 111.

[5] I. Tabushi, S. Kugimiya, *J. Am. Chem. Soc. 107* (1985) 1859.

[6] K. Ageishi, T. Endo, M. Okawara, *J. Polym. Sci. Chem. 21* (1983) 175.

[7] A. Factor, G. E. Heinsohn, *J. Polym. Sci. Part B 9* (1971) 289.

[8] F. Kröhnke, J. Wolff, G. Jeutsch, *Chem. Ber. 84* (1951) 399.

[9] ^{1}H NMR spectrum of **3** (in CD_3OD): δ = 4.54 (2H; OH), 4.82 (2H; CH_2), 5.05 (2H; CH_2), 5.27 (1H). ABX system with J_{AB} = 15.8 Hz, J_{ax} = 8.0, J_{BX} = 3.1; CHOH), 7.32–7.51 (10H, m; C_6H_5), 8.67 (4H), 9.18 (4H, AA'BB' system with J_{AB} = 6.2 Hz). Voltammetric data of **3**: E_p(red) = −0.57, −0.94 V; E_p(ox) = −0.49, −0.87 V.—^{1}H NMR spectrum of **4** in [D_6]DMSO: δ = 7.53–7.66 (6H, m; *m*-, *p*-C_6H_5), 7.72–7.78 (4H, m; *o*-C_6H_5), 7.94 (0.44H), 8.43 (0.44H, AB system with J_{AB} = 14.2 Hz), 8.79 (0.88H), 9.53 (0.88H, AA'BB' system with J_{AB} = 6.6 Hz), 8.05 (1.56H), 8.51 (1.56H, AB system with J_{AB} = 14.5 Hz), 9.02 (3.12H), 9.70 (3.12H, AA'BB' system with J_{AB} = 6.6 Hz). UV spectrum of **4**: λ_{max} = 362 nm ($\varepsilon = 2.21 \times 10^4$).

[10] S. I. Imabashi, N. Kitamura, S. Tazuka, K. Tokuda, *J. Electroanal. Chem. 239* (1988) 397; T. W. Ebbesen, R. Akaba, K. Tokumaru, M. Washio, S. Tagawa, Y. Tabata, *J. Am. Chem. Soc. 110* (1988) 2147.

[11] C, H, N, Hal. analysis found (calculated): **1** $(C_{20}H_{16}Br_{1.66}Cl_{0.33}N_2)_n$, (428.7) × n: C 56.1(56.0), H 4.2(3.7), Br 20.5(30.9), Cl 1.8(2.7), N 5.5(6.5). **5** $(C_{20}H_{20}Br_2N_2O_2)_n$, (464.7) × n: C 50.2(50.0), H 5.0(4.2), Br 23.5(33.5), N 5.7(5.8).

[12] The carbon paste was prepared with DMSO solvent in an experimental arrangement as given in: P. Audebert, G. Bidan, *Synth. Metals 14* (1986) 71. We thank Dr. *P. Audebert* and Dr. *C. Andrieux*, University of Paris 7, for kind assistance in these experiments.

[13] L. J. van der Pauw, *Philips Techn. Rundsch. 20* (1958/1959) 220.

Probing Changes in the Structure and Performance of a Lithium Nickel Oxide Catalyst by in situ X-Ray Diffraction During the High-Temperature Oxidative Coupling of Methane**

By *Ingrid J. Pickering, Peter J. Maddox* and *John M. Thomas**

Heterogeneous catalysts and their precursors are customarily characterized under conditions profoundly different from those that prevail in the actual catalytic reaction. The active solid may possess structural features quite unlike those deduced from measurements conducted at ambient temperatures and pressures. This calls for the increased use of in situ methods for the characterization of heterogeneous

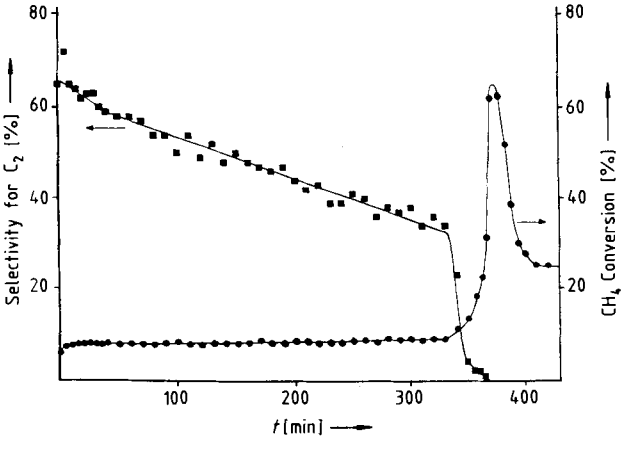

Fig. 1. The changes with time of conversion of methane and selectivity for C_2 hydrocarbons are shown for the duration of the experiment. Percentage conversion of methane is derived as $(100 \times \Sigma n V_{C_n})/V_{CH_4} + \Sigma n V_{C_n}$ and percentage selectivity for ethane and ethene as $(100 \times (2 V_{C_2H_6} + 2 V_{C_2H_4}))/\Sigma n V_{C_n}$ where V_{C_n} is the percentage volume of C_n hydrocarbon product (CO, CO_2, C_2H_4, C_2H_6) in the gas chromatographic analysis. (These values do not take into account any carbon which forms carbonate or other solid phases).

[*] Prof. Dr. J. M. Thomas, I. J. Pickering, Dr. P. J. Maddox
Davy Faraday Research Laboratory
The Royal Institution of Great Britain
21, Albemarle Street, London W1X 4BS (UK)

[**] We thank the Science and Engineering Research Council for a studentship (to *IJP*), a fellowship (to *PJM*) and an equipment grant (to *JMT*).

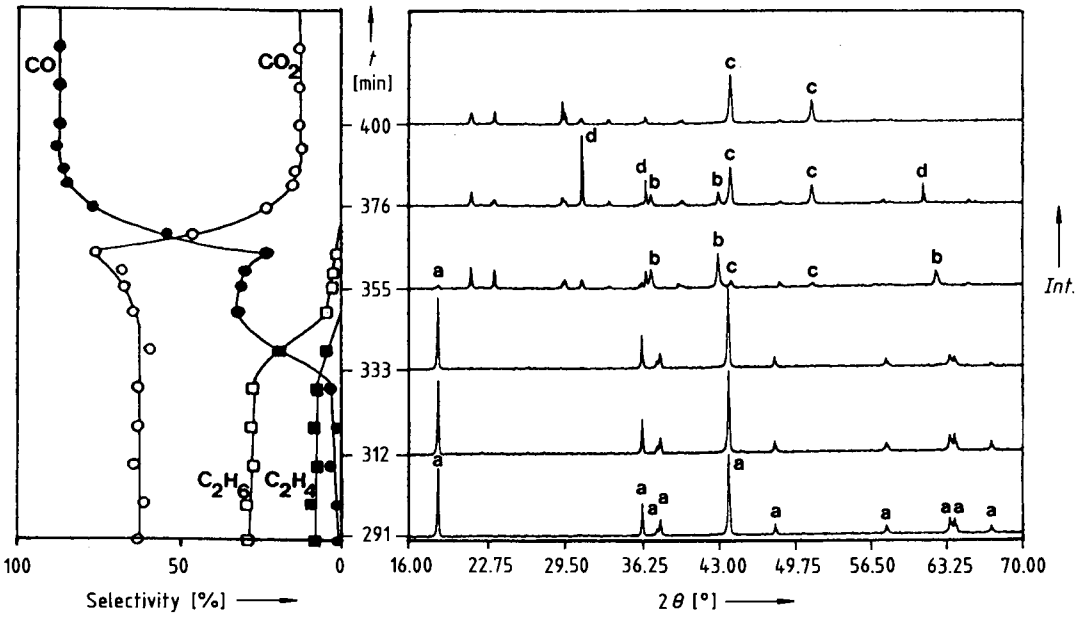

Fig. 2. Variation in selectivities and diffraction patterns as a function of time for the final stages of the reaction. Left: individual percentage selectivities for the various products. Right: corresponding in situ diffraction patterns of the catalyst. The vertical position of the diffraction pattern represents the time at which the scan was commenced, at 16° (2 θ). Diffraction peaks labelled as follows: a: $Li_{0.45\pm0.02}Ni_{0.55\pm0.02}O$, b: NiO, c: Ni metal and d: unknown transient.

catalysts. Here we illustrate the advantages of in situ X-ray diffraction in clarifying the onset and nature of distinct kinds of catalytic action exhibited by a lithium nickel oxide for the oxidation of methane at elevated temperatures.[1, 2]

A sample of 1.01 g of the powdered solid of composition $Li_{0.45\pm0.02}Ni_{0.55\pm0.02}O$ was placed in a porous quartz sample holder in a specially-constructed, resistively-heated, quartz reaction cell fitted with mica windows.[3] The cell was attached to a slightly modified Siemens D500 diffractometer equipped with a rotating anode source (CuK_α radiation), which allowed rapid structural characterization. Under the flow of the reaction gas mixture (composition: CH_4 19.68%, O_2 3.00%, balance N_2; flowrate: 50 mL min^{-1}), the catalyst was rapidly heated to and maintained at 700 °C. A series of diffraction patterns was recorded (2 θ range 16 to 70°), each pattern requiring some 19 min, and concurrently the outlet product gases were analyzed by gas chromatography.

The conversion of methane, and the selectivity for C_2 hydrocarbons during the 7 h catalytic run are shown in Figure 1. After about 330 min the nature of the catalysis changes dramatically (see also expanded version with the appropriate diffraction patterns in Fig. 2). It should be noted that there are three distinct regimes of catalysis associated with correspondingly distinct structural features.

During the initial regime (up to 330 min) the fractional conversion of methane remains essentially constant at ca. 8%; concomitantly the selectivity of C_2 products starts at 65% and gradually drops, for reasons that are at present obscure, to a value of 33% at t = 330 min. The diffraction patterns reveal that a single phase, lithium nickel oxide, functions as the oxidative coupling catalyst. The structure,[4] schematized in Figure 3a, is of the rocksalt type with different cation distributions on alternate close-packed layers.

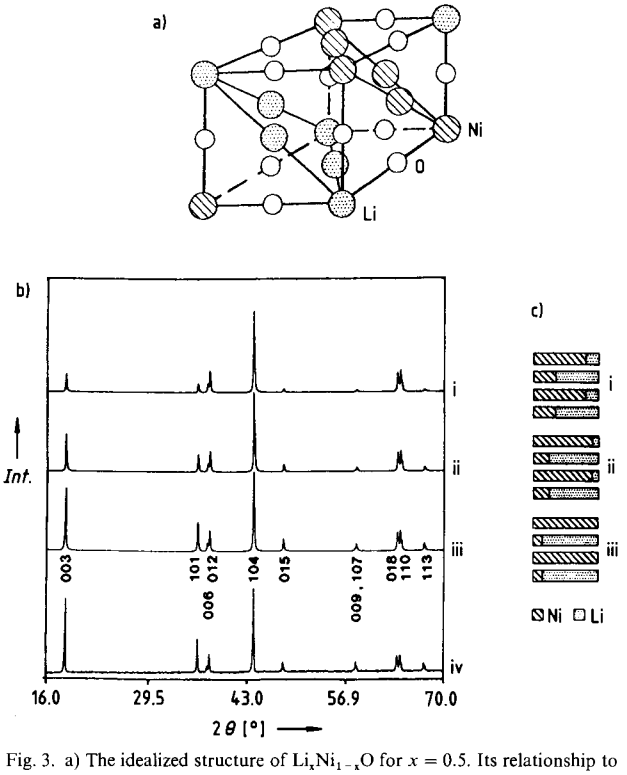

Fig. 3. a) The idealized structure of $Li_xNi_{1-x}O$ for x = 0.5. Its relationship to the rocksalt structure is shown, lithium and nickel ions occupy alternate close-packed layers between the oxygens. b) Diffraction patterns of $Li_xNi_{1-x}O$ for x = 0.43. i, ii and iii are simulated diffraction patterns for increasing order between the layers. Lattice parameters for the simulations are taken from the experimental data (a = 2.905, c = 14.361 Å). iv is the first experimental diffraction pattern collected at reaction temperature (700 °C). c) Representation of the ordering of Li and Ni between the layers. i, ii and iii are the models for i, ii and iii in part b, respectively. i has 20% Li in the predominantly Ni layer, 66% in the other layer; likewise ii 10 and 76%; iii 0 and 86%, i.e. totally ordered.

Diffraction patterns have been simulated (Fig. 3 b, i to iii) for different degrees of ordering[5] of lithium and nickel ions between the layers (represented in Fig. 3 c, i to iii). Comparison with the initial diffraction pattern at 700 °C (Fig. 3 b, iv) shows that the lithium ions are essentially fully ordered between the layers. The unit cell is hexagonal, $R\bar{3}m$ with computed cell dimensions of $a = 2.904$ and $c = 14.36$ Å with a slight axial distortion away from the true cubic close packing ($c/a = 4.945$; ideal cubic = 4.899). This distortion is greater than at room temperature ($a = 2.885$, $c = 14.21$ Å, $c/a = 4.925$). The Figures 2 and 3 show that, during the initial period of catalytic activity the lithium nickel oxide structure remains invariant within the limits of our technique. The oxide appears to function as a uniform heterogeneous catalyst in the sense previously elaborated.[6]

In the second regime, 330–360 min, there is dramatic change; at least two crystallographic phases are present as the parent $Li_{0.46}Ni_{0.54}O$ is reduced to its daughter phase NiO (labelled b in Fig. 2). Accompanying the appearance of NiO there is a sharp rise in the degree of conversion of CH_4, and the principal product is CO_2. Production of C_2 hydrocarbons decreases to zero as the Li-Ni-O phase disappears.

In the third and final regime, 360 min and longer, metallic nickel (c in Fig. 2) along with some Li_2CO_3, is the predominant crystallographic phase. It is also noted that new, sharp peaks appear (labelled d); these are as yet unidentified and rapidly disappear (see top diffraction pattern of Fig. 2) before the catalyst is finally converted to metallic nickel and lithium carbonate. In this regime CO is the dominant gaseous product of catalytic reaction, and there is now no longer a uniform heterogeneous catalyst.

In summary, it has been shown that in situ X-ray diffractometry coupled with parallel gas chromatography throws fresh light on the structure of reactive solid catalysts. In the case of the Li-Ni-O system studied here, three distinct regimes could be readily identified each with different gaseous products. Furthermore, although the experimental conditions were not optimized, it was possible to detect the presence of an as yet unidentified transitory solid product as well as those expected on the basis of the known chemistry of the parent, monophasic mixed oxide catalyst. Greater time resolution may be attained with our set-up by using a higher flux of X-rays and a more sensitive detector.

Received: January 30, 1989

[1] M. Hatano, K. Otsuka, *Inorg. Chim. Acta 146* (1988) 243–247.
[2] R. K. Ungar, X. Zhang, R. M. Lambert, *Appl. Catal. 42* (1988) L1–L4.
[3] P. J. Maddox, J. Stachurski, J. M. Thomas, *Catal. Lett. 1* (1988) 191.
[4] L. D. Dyer, B. S. Borie, Jr., G. P. Smith, *J. Am. Chem. Soc. 76* (1954) 1499.
[5] J. B. Goodenough, D. G. Wickham, W. J. Croft, *J. Phys. Chem. Solids 5* (1958) 107.
[6] J. M. Thomas, *Angew. Chem. Int. Ed. Engl. 27* (1988) 1673; *Angew. Chem. 100* (1988) 1735.

The following short communications will be published in future issues: *D. Schweitzer et al:* Superconductivity at 7.5 K and Ambient Pressure in Polycrystalline Pressed Samples of β_p-(BEDT-TTF)$_2I_3$ – *R. Kniep et al:* Structure of Anodic Oxide Coatings on Aluminum – *G. Gray et al:* Siloxane Copolymers with Laterally and Terminally Attached Mesogenic Side Chains

High Resolution Electron Microscopy of the High-T_c Superconductor $Bi_{2+x}Sr_2Ca_{1-x}Cu_2O_{8+\delta}$

By *W. Zhou, A. I. Kirkland, K. D. Mackay, A. R. Armstrong, M. R. Harrison, D. A. Jefferson, W. Y. Liang* and *P. P. Edwards**

The structure of the 85 K Bi-Sr-Ca-Cu-O superconductor has been investigated by means of high resolution electron microscopy combined with image simulation. An ordered one-in-five substitution of calcium by bismuth ions is proposed as the explanation for the observed superlattice formation. This model is consistent with the reports of the recent analytical studies carried out on the same system.

The discovery of high temperature superconductivity in the Bi-Sr-Ca-Cu-O system has demonstrated conclusively that this phenomenon is not confined to compounds containing yttrium and rare-earth elements.[1–4] Several groups have isolated a high-T_c phase in this system and single crystal X-ray[4–6] and neutron diffraction[7] studies have shown both similarities and differences between these new cuprate superconductors and the previously known 40 K and 90 K materials.[4–6] A superstructure has also been observed in these diffraction studies and various structural models for its formation have been proposed.[8–10] Equally important was the indication of additional electron density at the Ca site suggesting a variable Bi:Sr:Ca occupancy.[5,6] Here the results of high resolution electron microscopy (HREM) and model image simulation of the title compound are presented from which an ordered compositional variation in atomic arrangement, which leads naturally to the superlattice for-

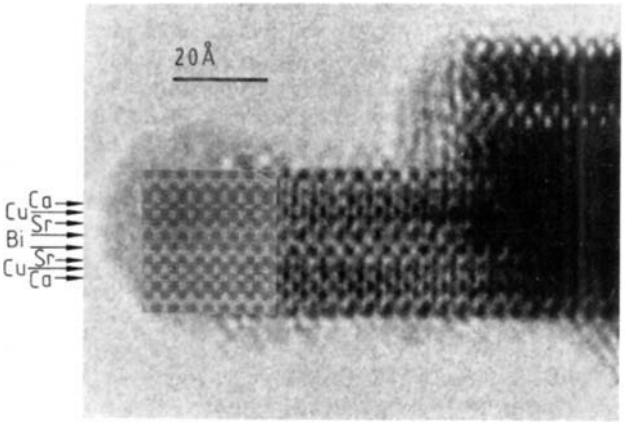

Fig. 1. HREM image of the tip of one crystal a single c lattice vector wide viewed down [110] of the published unit cell together with a calculated image inset (defocus = 950 Å, crystal thickness = 20 Å). The image clearly shows in cross section the metal layers in the order (Bi-Sr-Cu-Ca-Cu-Sr-Bi).

[*] Dr. P. P. Edwards, Dr. W. Zhou, Dr. A. I. Kirkland, Dr. K. D. Mackay, Dr. A. R. Armstrong, Dr. D. A. Jefferson, Dr. W. Y. Liang
Interdisciplinary Research Centre in Superconductivity
University of Cambridge
Madingley Road, Cambridge CB3 0HE (UK)
Dr. M. R. Harrison
General Electric Company
Hirst Research Centre
East Lane, Wembley, Middlesex HA9 7PP (UK)

[**] We thank the SERC, P.A. Technology (*W. Z.*), Alcan Chemical Ltd. (*A. I. K.*), and B.P. Research (*A. R. A.*) for financial support.